Analyst

Cite this: *Analyst*, 2012, **137**, 3011

www.rsc.org/analyst

PAPER

Real-time characterization of cytotoxicity using single-cell impedance monitoring†‡

Fareid Asphahani,[a] Myo Thein,[b] Kui Wang,[a] David Wood,[a] Sau Shun Wong,[a] Jian Xu[b] and Miqin Zhang*[a]

Received 9th November 2011, Accepted 2nd March 2012
DOI: 10.1039/c2an16079j

Cellular impedance sensors have attracted great attention as a powerful characterization tool for real-time, label-free detection of cytotoxic agents. However, impedance measurements with conventional cell-based sensors that host multiple cells on a single electrode neither provide optimal cell signal sensitivity nor are capable of recording individual cell responses. Here we use a single-cell based platform to monitor cellular impedance on planar microelectrodes to characterize cellular death. In this study, individual cells were selectively patterned on microelectrodes with each hosting one live cell through ligand-mediated natural cell adhesion. Changes in cellular morphology and cell–electrode adherence were monitored after the patterned cells were treated with varying concentrations of hydrogen peroxide, sodium arsenite, and disodium hydrogen arsenate, three potent toxicants related to neurotoxicity and oxidative stress. At low toxicant concentrations, impedance waveforms acquired from individual cells showed variable responses. A time- and concentration-dependent response was seen in the averaged single-cell impedance waveform for all three toxicants. The apoptosis and necrosis characterizations were performed to validate cell impedance results. Furthermore, time constants of apoptosis and necrosis in response to toxicant exposure were analytically established using an equivalent circuit model that characterized the mechanisms of cell death.

Introduction

In vitro cytotoxicity testing is an important research protocol in drug development and assessment of potentially harmful chemicals.[1–4] When subjected to a toxic substance, cells undergo changes in morphology and adherence.[5,6] Many cell-based assays have been developed on a microchip platform to characterize these responses, enabling high-throughput cytotoxicity screening.[7,8] Yet, the cytotoxic response of individual cells can be highly variable. Single-cell biosensors make it possible to study heterogeneous properties of the toxic response of individual cells that are otherwise masked within the averaged response of a cell population.[9]

Cellular impedance biosensors can be constructed for real-time, nondestructive, label-free detection and analysis of cytotoxic agents and their temporal effects.[10,11] Cell impedance measurements monitor electrical alternations between the cell and electrodes either at the interface where cells adhere to planar microelectrodes or dynamically in motion through microfluidic channels.[12] To date, cell impedance sensors have been employed to study the cytotoxic effects of a wide variety of substances, such as steroids,[13] air particulates,[14] drinking water contaminants and disinfectants,[15,16] nanoparticles,[17–19] and other organic and inorganic chemicals,[20–23] and have compared favorably to conventional cytotoxicity assays.[24,25] The conventional cell-impedance sensors generally study the behavior of multiple cells on large-sized electrodes and provide data on the collective response of cells to a given physiological condition. Furthermore, few studies[26,27] have investigated the cytotoxic effects on single cells using the impedance technique due to the technical challenges in isolating and seeding of individual cells on IMA platforms and producing a sufficient cell signal-to-noise ratio (SNR).[10]

We recently developed a multimodal (optical and electrical) single-cell impedance monitoring system built upon an integrated microelectrode array (IMA)-based chip.[28] Individual cells were patterned on the IMA chip through ligand-mediated natural cell adhesion for tight cell–electrode attachment, which maximized SNR[29] and maintained viability and normal functionality of patterned cells.[30] In this system, the influence of cell-to-cell interactions was excluded and only the true response to drug or toxin by the cell was accurately measured.[31] The electrical signals measured from a single cell on an electrode were shown to be superior to multiple cells placed on a common electrode because

[a]*Department of Materials Science & Engineering, University of Washington, 302L Roberts Hall, Seattle, Washington, 98195-2120, USA. E-mail: mzhang@u.washington.edu; Tel: +1 206 616-9356*
[b]*Department of Engineering Science and Mechanics, Pennsylvania State University, University Park, PA 16802, USA*

† This article is part of a themed issue highlighting the targeted study of single units, such as molecules, cells, organelles and pores – The "Single" Issue, guest edited by Henry White.

‡ Electronic supplementary information (ESI) available. See DOI: 10.1039/c2an16079j

shunt current paths and more cell-to-electrode separation exist for a larger electrode hosting multiple cells.[29] Single-cell impedance was dependent upon the degree of alteration in cell morphology and attachment on the detecting electrode. It is found that better cell coverage and tight cell–electrode contact result in significantly larger change in measured signal for the same degree of cellular response.[29] Hence, a single-cell MEA chip renders highly sensitive and robust cellular signals in cell-based biosensors and assay platforms for drug screenings. Unlike most conventional cytotoxicity assays that can only provide results of specific cellular changes (*e.g.*, viability) at distinct time points after toxicant exposure, this IMA system is well suited to study the cytotoxic effect on single cells over time. Therefore, we hypothesize that single-cell impedance waveforms acquired under the influence of a toxicant can provide fundamental information about the physiological and pathological responses of individual cells in addition to their collective response.

This study investigated the use of single-cell impedance monitoring to assess the cytotoxicity of toxic compounds on live cells, with hydrogen peroxide (H_2O_2), sodium arsenite ($NaAsO_2$), and disodium hydrogen arsenate (Na_2HAsO_4), as model toxicants, and a human malignant glial cell line (T98G) as model cells. Chemicals that interact with the nervous system may put neuronal functions at risk as they may interfere with general biochemical properties or specific neuronal structures and processes. Glial cells are susceptible to toxins found in the environment, such as arsenic-based compounds, a potential source of neurotoxins,[32] which are known to interact with the nervous system in a manner that inhibits locomotor function and can be lethal at high concentrations.[33] Reactive oxidative species (ROS), such as hydrogen peroxide (H_2O_2), has been suggested to be one cause of neurodegenerative diseases such as Alzheimer's and Parkinson's diseases.[34] Cell apoptosis–necrosis staining assays were performed to validate cell impedance results. An equivalent electric circuit model was developed to determine the time constants of cell death resulting from apoptosis and necrosis for each concentration of the tested toxicants.

Experimental

Chemicals and materials

The following materials and chemicals were used as received: Remover PG (MicroChem, Newton, MA); 1-octanethiol 98.5%, 3-mercaptopropionoic acid 95% (3-MPA), hydrochloric acid (HCl) 37%, *N*-hydroxysuccinimide 97% (NHS), sodium arsenite ($NaAsO_2$), disodium hydrogen arsenate (Na_2HAsO_4), and 1-ethyl-3-(3-(dimethylamino)-propyl) carbodiimide (EDAC) (Sigma-Aldrich, Milwaukee, WI); hydrogen peroxide (H_2O_2) (Mallinckrodt Baker, Phillipsburg, NJ); 2-[methoxy(polyethyleneoxy)propyl] trimethoxysilane (PEG) of M_w = 460–590 Da (Gelest, Morrisville, PA); 1× Phosphate Buffered Saline (PBS) solution, Opti-MEM® I Reduced-Serum Medium (O-MEM), Dulbecco's Modified Eagle's Medium (DMEM), fetal bovine serum (FBS), penicillin–streptomycin–neomycin (PSN) antibiotic 100× mixture, TrypLE™ Express Stable Trypsin Replacement, Alexa Fluor 488-conjugated wheat germ agglutinin (WGA; W11261), and ProLong® Gold antifade reagent with DAPI (Invitrogen, Carlsbad, CA); and lysine–arginine–glycine–aspartic acid (KRGD) oligopeptide (RS Synthesis, Louisville, KY). All the solvents including toluene, isopropanol, and xylenes were HPLC grade and were purchased from Sigma-Aldrich. For the cell viability assay, the Apoptotic & Necrotic & Healthy Cells Quantification Kit (30018) was used (Biotium, Hayward, CA). Absolute ethanol was always deoxygenated by dry N_2 before use. T98G human glioblastoma multiforme cells were obtained from the American Type Culture Collection (Manassas, VA).

IMA surface modification

IMA substrates were fabricated in the same manner as previously reported[28] and chemically modified based on previously established surface modification procedures[28,29,35] that are summarized herein. The IMA substrate design has electrodes of 30 μm diameter to host single cells and of 250 μm diameter to host multiple cells, and two large, rectangular counter electrodes with negligible electrode impedance. The gold/silicon oxide substrates of the IMA chip were first washed with Remover PG, isopropanol, ethanol, and DI water, respectively, to remove the protective photoresist layer. The substrates were then placed in a Bioforce ProCleaner™ UV/ozone chamber (BioForce Nanosciences, Des Moines, IA) for 60 min, after which they were rinsed thoroughly with ethanol, and placed in a 0.1 mM 1-octanethiol solution in ethanol for 16 h to form a self-assembled monolayer (SAM) over the gold electrodes. The silicon background was passivated with PEG solution prepared in a nitrogen environment by adding 3 mM PEG in anhydrous toluene containing 0.1% concentrated HCl at room temperature for 18 h. Following the PEG reaction, the 1-octanethiol SAM was removed from the gold electrodes by heating in xylenes solvent at 120 °C for 2 h and sonicating the surfaces in xylenes and ethanol, respectively, for 5 min each to dispel loosely bound moieties. The gold electrodes were reacted with a 20 mM 3-MPA carboxylic acid-terminated alkanethiol for 16 h at room temperature. For surfaces to be covalently linked with KRGD oligopeptide biological ligands, substrates were immersed in an aqueous solution of 150 mM EDAC and 30 mM *N*-hydroxysuccinimide (NHS) for 30 min to attach the NHS ester intermediate to activate carboxylate groups of the 3-MPA to chemically bond primary amino groups of KRGD. The substrates were submerged in a 50 μg mL^{-1} KRGD solution in PBS buffer of 8.2 pH at room temperature for 1 h. To remove loosely bound moieties after each step of the surface modification, the substrate was rinsed with its original buffer solution and DI water.

Cell seeding on IMA chips

A human glioblastoma multiforme cell line (T98G) was cultured in 75 cm^2 flasks at 37 °C in a humidified atmosphere with 5% CO_2 using DMEM cell culture medium containing 10% FBS and 1% PSN antibiotic and supplemented with 4 mM L-glutamine, 1.5 g L^{-1} sodium bicarbonate, and 4.5 g L^{-1} glucose. The medium was changed every third day. For cell adhesion on IMA chips, the culture medium was changed to O-MEM containing the same supplements, and T98G cells were seeded at a concentration of 2×10^3 cells mL^{-1} onto the peptide-patterned IMA substrates.

The cells were allowed to adhere to the electrodes for 24 h under standard culture conditions.

Electrical measurements of cell response

Cell-hosting IMA substrates were housed inside a portable microchip carrier integrated to a multiplexer relay switching system (MUX). Preamplification circuitry was built on a printed circuit board (PCB). The IMA chip carrier – MUX/preamp PCB was placed under an upright microscope (Nikon 80i, Melville, NY) encased within a cell incubator chamber to maintain a controlled temperature and airflow environment. The MUX/preamp PCB was connected to a Stanford Research Systems SR810 lock-in amplifier (Sunnyvale, CA). The MUX/preamp PCB served as both the input waveform generator and output signal analyzer. Data acquisition and channel switching were controlled by a PC through a GPIB interface using LabVIEW software (National Instruments, Austin, TX).

Cellular impedance measurements were taken in the following manner. The input signal of a 22 mV (peak-to-peak) sine wave at a frequency of 2 kHz was passed through a 220 kΩ resistor in a voltage divider circuit to limit the current amplitude to 100 nA. The 2 kHz frequency was selected for single-cell impedance measurements because this frequency has been shown to generate the largest cell-to-baseline signal for this IMA impedance system.[28] Electrical characterization involved measuring the voltage amplitude between the detecting electrode and counter electrode (ΔV) and the signal phase shift ($\Delta\varphi$) by use of the SR810 lock-in amplifier. Complex impedance was calculated and analyzed post-processing from the measured output voltage using MATLAB® software.

Cell impedance analysis of cytotoxicity

24 h after baseline single-cell–electrode measurements were made, the cell culture medium was replaced with a fresh medium in the control well and with a medium containing H_2O_2 at the concentrations of 50, 125, 500, 2500, and 5000 μM, and $NaAsO_2$ or Na_2HAsO_4 at the concentrations of 10, 20, 50, and 100 μM. Cell–electrode voltage data were continuously recorded in the presence of the toxicants for an additional 24 h. Optical differential interference contrast (DIC) images were acquired before and after the toxicant was administered.

Fluorescence imaging of cell membranes and nuclei

Cell-patterned substrates were fixed with 4% paraformaldehyde solution. Following fixation, cells were stained with Alexa Fluor 488-conjugated WGA (membranes) and 4′,6-diamidino-2-phenyindole (DAPI) (nuclei) according to the manufacturers' instructions. Fluorescent images were acquired using a Nikon 80i Eclipse upright microscope (Nikon, Melville, NY) equipped with DAPI, FITC, and TRITC.

Apoptosis assay using flow cytometry

The Apoptotic & Necrotic & Healthy Cells Quantification assay kit was used to determine the manner of cell death using Hoechst 33342 (Hoechst), ethidium homodimer III (EtD-III), and FITC-conjugated Annexin V (Annexin V) staining reagents by flow cytometry analysis. After 4, 12, and 24 h of H_2O_2 exposure, cell staining was carried out following the manufacturer's protocol. Fluorescence-activated cell sorter analysis was performed with a BD LSR II Flow Cytometer (BD Biosciences). Data were analyzed with FloJo software. Cells were categorized as viable, apoptotic, necrotic, or late stage apoptotic/necrotic. The final percentage of toxicant-specific apoptosis, necrosis, or late apoptosis/necrosis was calculated by subtracting the percentage of spontaneous apoptosis, necrosis, or late apoptosis/necrosis of the relevant controls from the categorized percentage of apoptosis, necrosis, or late apoptosis/necrosis, respectively, for each incubation time.

Safety

Hydrogen peroxide, sodium arsenite, and disodium hydrogen arsenate are severe toxicants to living things that must be handled with extreme care. H_2O_2 is an oxidizing agent and is considered as a highly reactive oxygen species (ROS). $NaAsO_2$ and Na_2HAsO_4 are both known carcinogens. When handling, inhalation or contact must be avoided; wearing a respirator and protective gloves, clothing, and safety glasses is recommended in the MSDS. Preparation and use of these chemicals are recommended in an exhaust hood equipped with ventilation, and their disposal is considered as hazardous waste.

Results and discussion

Single-cell impedance response to hydrogen peroxide

To evaluate the sensitivity of our single-cell impedance sensors in detecting cytotoxicity in a time- and concentration-dependent manner, we treated single T98G cells adhered to and fully spread over 30 μm detecting electrodes with varying concentrations of the oxidative stressor H_2O_2 and acquired impedance data. H_2O_2 is considered as one of the most potent reactive oxygen species (ROS) because it maintains a long half-life and is soluble in lipid and aqueous media.[36] Exposure to exogenous ROS beyond the capacity for their detoxification can result in the degradation of intracellular biochemicals leading to cellular dysfunction or death. These toxic effects monitored by cellular impedance monitoring are shown in Fig. 1, which shows the normalized real component of the complex impedance response of T98G single cells on 30 μm electrodes exposed to 0 (control), 50, 125, 500, 2500, and 5000 μM H_2O_2. Data were recorded from each electrode every 10 min and normalized to the data point 2 h prior to H_2O_2 exposure.

Each individual cell seen in Fig. 1b–f underwent a distinct response to H_2O_2 induced toxicity that was transduced by the IMA impedance sensor. The impedances of cells that were not exposed to H_2O_2 remained near constant over time (Fig. 1a). Cells that were exposed to higher concentrations of H_2O_2 (*e.g.*, 500, 2500, and 5000 μM) responded more uniformly in impedance changes, and showed a rapid impedance decline in the first 12 h (Fig. 1d–f). This rapid decline in impedance indicates cell death and detachment from the electrode.[24] An initial increase in impedance for a short period (within 1 or 2 h after initial exposure to H_2O_2) was observed for some of the cells. This phenomenon has also been previously observed in impedance toxicity measurements,[6,20,37] which is understood as cellular

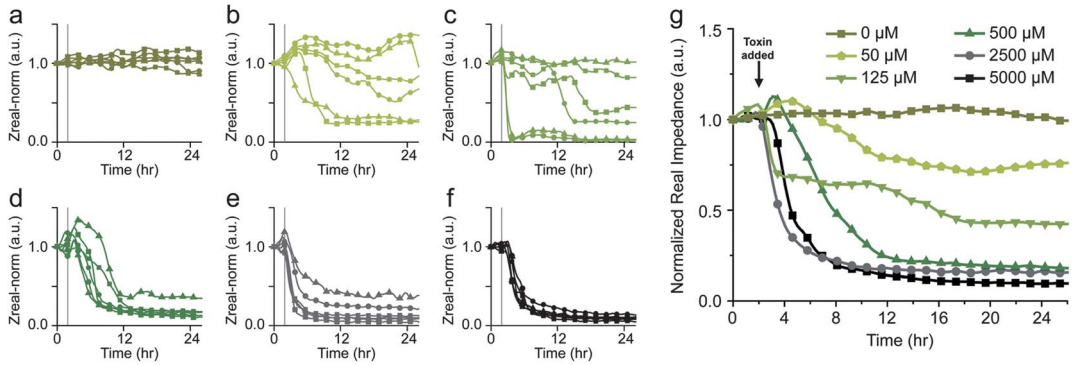

Fig. 1 (a–f) Time course graphs depicting the normalized real impedance waveforms of T98G single cells (6 cells per group × 6 groups) exposed to (a) 0, (b) 50, (c) 125, (d) 500, (e) 2500, and (f) 5000 μM of H_2O_2, respectively. The impedance waveform generated by each single cell was normalized to the respective impedance produced by the cell two hours prior to H_2O_2 inoculation at $t = 0$ h. Toxicant deposition was made at $t = 2$ h, which is denoted by a faded vertical line. (g) Time course graph of the averaged impedance waveforms of T98G single cells in response to concentrations of 0, 50, 125, 500, 2500, and 5000 μM of H_2O_2; each impedance waveform was generated by averaging the impedances of 6 cells in each group, representing the collective cellular response to a particular toxicant concentration.

volume increase initiated by the uptake of osmolytes due to the cell's inability to maintain ion homeostasis.[38]

For single cells exposed to the lower concentrations of H_2O_2 (*e.g.* 50 and 125 μM, Fig. 1b and c), impedance waveforms differ notably among individual cells in terms of both amplitude and rate of change. These variations suggest that the onset, duration, and manner in which cells underwent death were heterogeneous. The diverse responses among the cells in the same group exposed to a lower H_2O_2 concentration would not be discernible from the averaged impedance response (see Fig. 1g), which highlights the advantages of single-cell impedance analysis for identification of cell-to-cell variation.

Each impedance waveform shown in Fig. 1g was the averaged impedance waveforms generated by six individual cells in a group exposed to H_2O_2 of the same concentration, analogous to results obtained from a multi-cell impedance sensor. Exogenous H_2O_2 caused a decline in the average single-cell impedance ($Z_{sc\text{-}avg}$) at all H_2O_2 concentrations, but such declines demonstrated a concentration-dependent relationship.

For the control group (*i.e.*, cells not exposed to H_2O_2), no significant impedance change over time was seen, indicating that the single cells remained viable and firmly attached to the electrode.[28] For all other groups exposed to H_2O_2 of differing concentrations, different characteristics of impedance change were observed during the 24 h exposure period. While the most lethal concentrations (*e.g.*, 2500 and 5000 μM) of H_2O_2 induced a dramatic reduction of $Z_{sc\text{-}avg}$ within 1 h of exposure and the impedance signal reached 50% of the original strength within the first 3 h (*i.e.*, $t \leq 5$ h), the cells exposed to lower concentrations required more time to show a result. $Z_{sc\text{-}avg}$ for cells exposed to 500, 2500, and 5000 μM H_2O_2 settled to 18%, 16%, and 10% of the original signals, respectively, indicating that most of the cells had been completely killed and detached. For cells exposed to 50 μM H_2O_2, the $Z_{sc\text{-}avg}$ did not decrease until 4.8 h after exposure and reached a constant average of 76%. The 125 μM level did diminish the $Z_{sc\text{-}avg}$ below 50% of the original signal, but only after 13.4 h of H_2O_2 exposure. The signal of this concentration reached 42–43% after approximately 16 h. Fig. S1a in the ESI‡ shows optical DIC images depicting T98G single-cell morphological changes before and after 24 h of H_2O_2 exposure.

Assessment of apoptosis and necrosis

To provide the information on the manner of cell death, we chose to both qualitatively and quantitatively assess single T98G cells through optical imaging and flow cytometry. Fig. 2 shows fluorescent micrographs of single cells on electrodes 4 h after exposure to 0, 50, and 500 μM concentrations of H_2O_2. For the control (Fig. 2a), cellular membrane fluorescence shows that cells are well-spread covering the entire surface area of each electrode. However, the cellular coverage is notably reduced for most of the cells exposed to 50 μM H_2O_2 (Fig. 2b). For the higher H_2O_2 concentration of 500 μM, nearly half of the cells are detached from the electrodes (Fig. 2c).

Cells normally die by one of two major mechanisms: necrosis or apoptosis, which differ biochemically and morphologically.

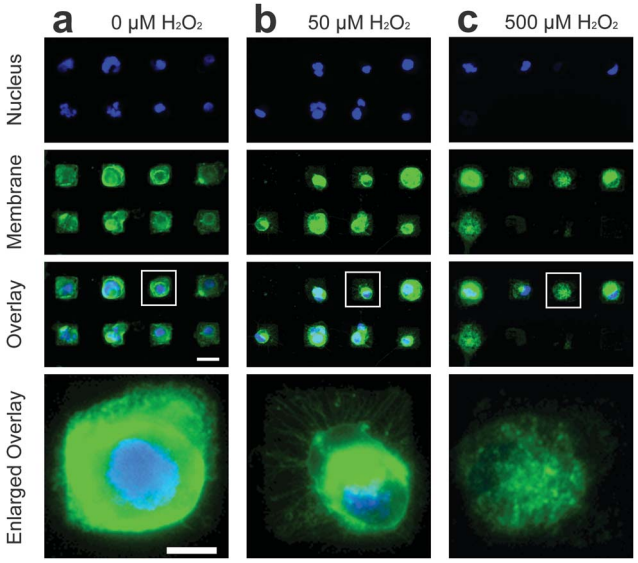

Fig. 2 Fluorescent micrographs of T98G cells patterned on an array of 30 μm square electrodes after 4 hours of treatment with (a) 0 μM, (b) 50 μM, and (c) 500 μM H_2O_2. The small scale bar is 30 μm, and the large scale bar is 10 μm.

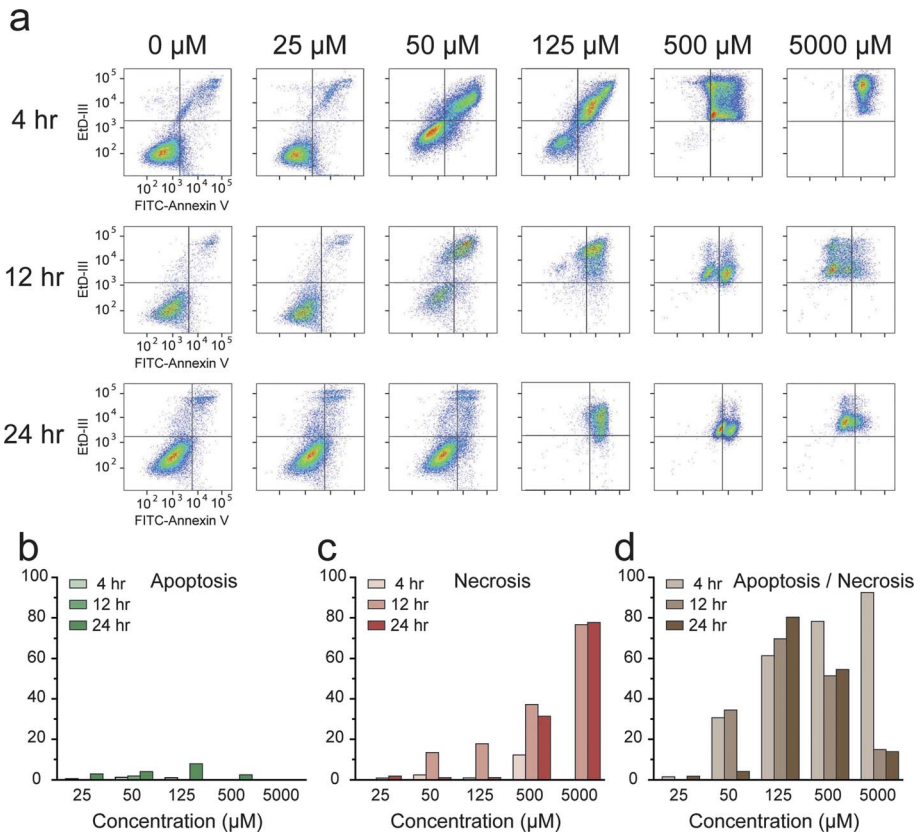

Fig. 3 (a) Flow cytometry profiles of T98G cells labeled with FITC-conjugated Annexin V and EtD-III and exposed to 25, 50, 125, 500, and 5000 μM H_2O_2 for 4, 12, and 24 h. Percent cell death due to toxicant-specific (b) apoptosis, (c) necrosis, and (d) late apoptosis/necrosis.

Necrosis is death due to cellular insult through external damage to the plasma membrane, which can happen in seconds. An initial increase in volume of a necrotic cell and plasma membrane lyses leads to the ultimate release of intracellular debris into the surrounding environment. Apoptosis is programmed cell death that consists of strictly regulated series of events that transpire much slower than necrosis, ranging from hours to days. Apoptosis is a naturally occurring phenomenon to eliminate damaged cells and maintain constant cell numbers, but can be triggered by external substances like ROS in lower concentrations. In apoptosis, there is a reduction in cell–substrate adhesion that typically results in a round cellular morphology, followed by zeiosis or surface blebbing, cell shrinkage, an outgrowth of echinoid-like extensions, surface membrane blistering, and eventual lysis.[39]

Early stage apoptotic characteristics, such as round morphology and echinoid-like extensions, can be observed from the stained plasma membranes, as shown by T98G subjected to 50 μM H_2O_2 (Fig. 2b). In addition, DAPI staining showed intact nuclear components (blue) for nearly all cells at this concentration, which was not the case for 500 μM H_2O_2 treatment where no or weak DAPI signals were detected from most of the electrodes (Fig. 2c). The latter result is consistent with the effects of necrosis, where membrane lysis results in the release of nucleic material into the culture media.

However, optical imaging of membrane morphology alone is not adequate to determine apoptosis from necrosis. One of the key hallmarks of apoptosis is that the phospholipid phosphatidylserine (PS) is translocated from the inner to the outer leaflet of the plasma membrane, while keeping the membrane intact. This prevents impermeable dyes, like propidium iodide or EtD-III, from entering the cell, which can determine whether or not the cell is necrotic. Since the protein Annexin V has a strong affinity to PS, a fluorescent dye conjugated to Annexin V can be used to identify apoptosis with microscopy or flow cytometry. Here, we used such staining to discern between apoptosis and necrosis of T98G using flow cytometry.

Fig. 3a shows the flow cytometric profiles of T98G cells labeled with FITC-conjugated Annexin V and EtD-III after treatment with 25, 50, 125, 500, and 5000 μM H_2O_2 for 4, 12, and 24 h. Cells were grouped into four subpopulations: (1) an Annexin V-negative/EtD-III-negative signal indicated viable cells; (2) an Annexin V-positive/EtD-III-negative signal was considered early stage apoptotic cells; (3) an Annexin V-negative/EtD-III-positive signal indicated necrotic cell death; and (4) an Annexin V-positive/EtD-III-positive signal denoted late-stage apoptosis with cell membrane damaged.[40] Fig. 3b–d show the percent cell counts for apoptosis, necrosis, and late apoptosis/necrosis for treatment with each of the H_2O_2 concentrations at the three exposure times.

Flow cytometry results identified that at lower H_2O_2 concentrations a sizeable population of cells survived for shorter exposure durations, while a small population of cells underwent apoptosis (Fig. 3b, showing 4.1% and 7.8% at 24 h for 50 and

125 μM H_2O_2, respectively). Apoptotic cell death corresponds to a gradual decline in impedance waveform exhibited by the single cells (Fig. 1b and c). Likewise, cell death due to membrane integrity loss was determined by flow cytometry (Fig. 3c and d), which corresponds to the rapid decline in impedance waveform among other single cells monitored by the impedance technique. For the 500 and 5000 μM concentrations, necrosis or late apoptosis/necrosis were the dominant pathways for cell death (Fig. 3c and d), which corresponds to a rapid reduction in impedance magnitude (Fig. 1d–f).

Impedance modeling of cytotoxic response of single cells

To examine the ability of single-cell impedance monitoring to identify the type of cell death, a single-cell–electrode model was proposed. The equivalent circuit model (ECM) of a single-cell covered planar electrode was based on models established elsewhere[28,31] in order to further analyze the relationship between $Z_{sc\text{-}avg}$ waveforms and the mechanisms of cell death. Cell death caused by apoptosis assumed retraction of cell coverage on the electrode until complete cell detachment, whereas necrosis assumed disruption of membrane dielectric integrity. The ECM was used to determine time constants for each of these cell death mechanisms at each concentration of a particular toxicant. For this ECM, H_2O_2 was used, and its experimental data were used to fit the model. Our approach assumed that the electrode's initial degree of cell coverage was at its maximum value, and overall impedance was normalized.

Time constants of induced cellular apoptosis. Cell retraction or shrinkage on the electrode due to induced apoptosis is the basis of this analysis. The radius of the spread cell, r_c, reduces to approximately 65.0% of its initial radius, r_c^0. This corresponds to the reduction in its averaged radius by 19.4%. Here, the initial radius of the cell is assumed to be equal to that of the electrode. The decay rate is estimated to be first order since the time course of apoptosis exhibits first order characteristics[40,41] and the cell radius decays to a steady-state limiting value r_c^∞. Mathematically, the rate of change of cell's radius can be described by eqn (1) at time t:

$$\frac{dr_c(t)}{dt} = -\frac{1}{\tau_n}\left[r_c(t) - r_c^\infty\right]. \quad (1)$$

The initial condition is $r_c^0 = r_e$ at $t = 0$, and the steady-state condition is $r_c^\infty = 0.81 r_e$ at $t = \infty$.

Solving eqn (1) by separation of variables and applying initial and steady-state conditions, the time-dependent cell radius during induced apoptosis (*i.e.*, H_2O_2 toxic effects) is given by eqn (2):

$$r_c(t) = r_e[0.19e^{-t/\tau_a} + 0.81], \quad (2)$$

where τ_a is the characteristic time (or time constant) of apoptosis due to H_2O_2 toxic effects.

Time constants of induced cellular necrosis. The integrity of the cell membrane is compromised due to H_2O_2 toxicity-induced necrosis. Therefore, the impedance of the cell membrane reduces over time during cellular necrosis (or the resistivity of the cell (ρ_c) reduces over time due to cell membrane breakdown). The decay rate is assumed to be logistic since time course disruption of cell membrane integrity during necrosis, which is represented by the release of intracellular lactate dehydrogenase (LDH) into the extracellular medium[42] and formation of blebs,[43] exhibits sigmoidal characteristics. Mathematically, the rate of change of a cell's resistivity can be described by eqn (3), with characteristic time τ_n:

$$\frac{d\rho_c(t)}{dt} = -\frac{1}{\tau_n}\left[1 - \frac{\rho_c(t)}{1/\tau_n\alpha}\right]\rho_c(t). \quad (3)$$

In this case, the initial condition is $\rho_c = \rho_c^0$ at $t = 0$, while at steady state $\rho_c \cong 0$ at $t = \infty$.

Solving eqn (3) by separation of variables and the use of partial fraction expansion with the application of initial and steady-state conditions, the time-dependent resistivity of the cell during necrosis is given by eqn (4):

$$\rho_c(t) = \frac{(1/\tau_n\alpha)\rho_c^0}{\rho_c^0 + \left[(1/\tau_n\alpha) - \rho_c^0\right]e^{t/\tau_n}}, \quad (4)$$

where τ_n is the characteristic time of necrosis and α is a constant whose value must satisfy the following condition in order to represent the decay:

$$0 < \rho_c^0 < \frac{1}{\tau_n\alpha}. \quad (5)$$

A summary of the time constants for apoptosis and necrosis is presented in Table S1 (ESI‡). Shorter time constants correspond to the necrotic cell death. The estimated time constants for H_2O_2 toxicity show that with higher dosages of toxicant, necrosis is the dominant mechanism in triggering the cell death.

Modeling of cell–electrode impedance. The single-cell–electrode structure in this study has the following properties: (1) the electrode possesses cell-occupied area A_c and cell-free area $A_{free} = A_e - A_c$ (where A_e is the area of the electrode); (2) cell adhesion is strong due to surface mediated cell adhesion, represented by a very large R_{seal}; and (3) the overall electrical impedance of single-cell–electrode heterostructure changes over time due to H_2O_2 toxicity effects. In other words, cell's radius r_c and resistivity ρ_c change simultaneously over time. The time-dependent impedance of single-cell–electrode structure is given by eqn (6).

$$Z(j\omega,t) = \left[\left(Z_{e,c}(j\omega,t) + \frac{Z_c(j\omega,t)R_{seal}(t)}{Z_c(j\omega,t) + R_{seal}(t)}\right)^{-1} + \frac{1}{Z_{e,free}(j\omega,t)}\right]^{-1} + R_{soln}, \quad (6)$$

where $Z_{e,c}(j\omega,t)$ is the surface impedance of the electrode area occupied by the cell and is given by

$$Z_{e,c}(j\omega,t) = \frac{\left(\frac{1}{\rho_e} + j\omega c_e\right)^{-1}}{\pi[r_c(t)]^2}, \quad (7)$$

$Z_{e,free}(j\omega,t)$ is the surface impedance of cell-free electrode area and given by equation

$$Z_{e,free}(j\omega, t) = \frac{\left(\frac{1}{\rho_e} + j\omega c_e\right)^{-1}}{\pi\left\{r_e^2 - [r_c(t)]^2\right\}}, \quad (8)$$

$Z_c(j\omega, t)$ is the impedance of cell and given by equation

$$Z_c(j\omega, t) = \frac{\rho_c(t) - j[1/\omega c_c]}{\pi[r_c(t)]^2}, \quad (9)$$

$R_{seal}(t)$ is the impedance of sealed resistance and given by equation

$$R_{seal}(t) = \lim_{r' \to 0} \frac{\rho'_{soln}}{2\pi h} \int_{r'}^{r_c(t)} \frac{1}{r} dr, \quad (10)$$

R_{soln} is the spreading resistance and given by equation

$$R_{soln} = \frac{\rho_{soln}}{4r_e}, \quad (11)$$

and h is the distance between the cell and electrode. The theoretical time-dependent normalized real impedance given by eqn (12) was derived from the preceding equations and used to access the toxicity effects of H_2O_2 on the cell over time:

$$\text{Normalized Real Impedance} = \text{Re}\left[\frac{Z(j\omega, t) - Z^{ss}(j\omega)}{Z(j\omega, t_0) - Z^{ss}(j\omega)}\right] \quad (12)$$

where $Z^{ss}(j\omega)$ is the steady-state impedance of single-cell–electrode heterostructure. Normalized Real Impedance as a function of time is plotted in Fig. 4 and fits to the experimental data.

Single-cell impedance response to arsenic toxicants

To further evaluate our impedance sensors to assess cytotoxicity, we deposited arsenic in the form of $NaAsO_2$ and Na_2HAsO_4 into IMA cell culture media and acquired T98G single-cell impedance data in real time. These toxic effects monitored by impedance are presented in Fig. 5 and 6, respectively. Similar to cells exposed to H_2O_2, individual cell impedances were also characterized by a variety of waveform progressions due to $NaAsO_2$ toxicity, particularly at the lower 10 and 20 μM concentrations (Fig. 5a and b). But unlike the uniform single-cell impedance response monitored at higher H_2O_2 concentrations, the distinctive responses of individual cells exposed to 50 and 100 μM $NaAsO_2$ were heterogeneous and demonstrated temporal effects of cell death (Fig. 5c and d). Fig. 5e shows the $Z_{sc\text{-}avg}$ waveforms of T98G exposed to $NaAsO_2$, showing a time- and concentration-dependent relationship. Interestingly, none of the $NaAsO_2$ concentrations result in $Z_{sc\text{-}avg}$ waveforms declining to a signal value below 50% of the original impedance within 24 h of exposure. This trend can be better understood by examining complementary optical DIC images depicting T98G single-cell morphology before and 24 h after exposure to both arsenic-based toxicants in Fig. S1b and c (ESI‡). These images show that fragments of the cell membrane still cover the electrode after 24 h of exposure to either $NaAsO_2$ or Na_2HAsO_4.

For cells exposed to Na_2HAsO_4, impedances of individual cells exhibited a more uniform cellular response to both low and high Na_2HAsO_4 concentrations. 10 μM Na_2HAsO_4 induced no discernible change in cellular impedances for any of the single cells present (Fig. 6a), while 20 μM Na_2HAsO_4 resulted in only slight reductions in impedance for two of the six monitored cells (Fig. 6b). However, for higher concentrations of 50 and 100 μM, all individual cell impedances declined to a signal value ranging between 12% and 48% of their initial values (Fig. 6c and d). Additionally, the averaged single-cell impedance response (Fig. 6e) showed greater sensitivity in detecting cell death due to Na_2HAsO_4 toxicity (as low as 50 μM in this study) than a multi-cell hosting electrode based on

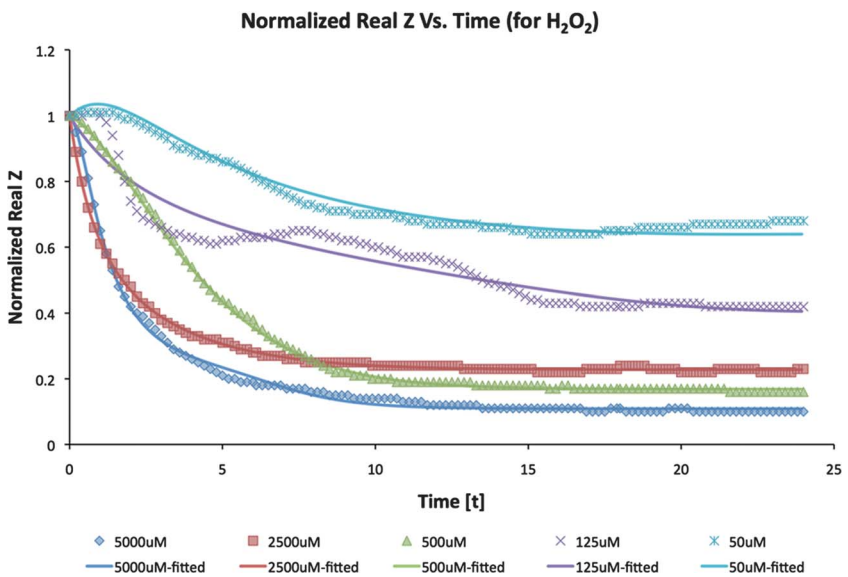

Fig. 4 Fitted, normalized single-cell real impedance plots from theoretical modeling (solid lines) and experimental impedance waveforms (broken lines) of T98G cells exposed to 50, 125, 500, 2500 and 5000 μM H_2O_2.

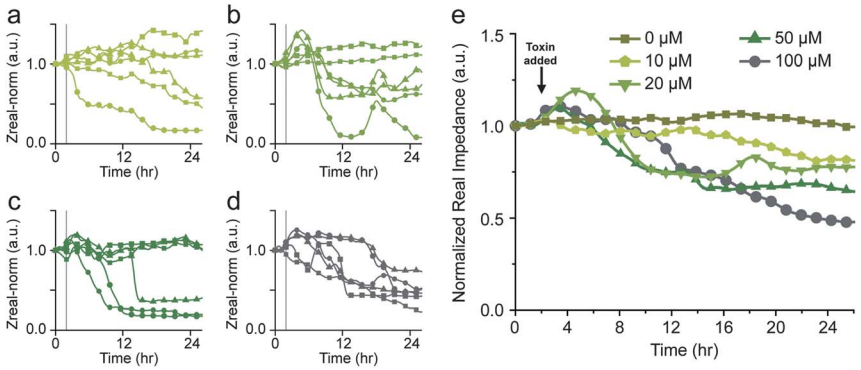

Fig. 5 (a–d) Time course graphs of the normalized real impedance waveforms of T98G single cells exposed to (a) 10, (b) 20, (c) 50, and (d) 100 μM of $NaAsO_2$, respectively. Six single-cell waveforms per group were recorded for each $NaAsO_2$ concentration. The real impedance was normalized to the impedance value two hours prior to $NaAsO_2$ inoculation ($t = 0$ h), and toxicant deposition was made at $t = 2$ h (denoted by the faded vertical line). (e) Time course graphs of the averaged real impedance waveforms of T98G single cells exposed to 0, 10, 20, 50, and 100 μM of $NaAsO_2$.

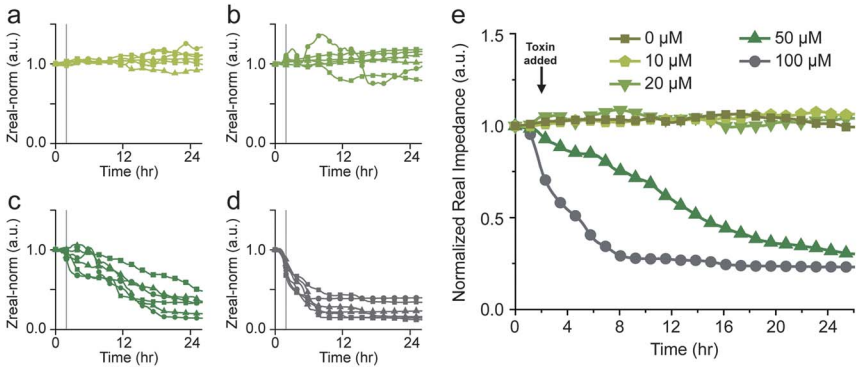

Fig. 6 (a–d) Time course graphs of the normalized real impedance waveforms of T98G single cells exposed to (a) 10, (b) 20, (c) 50, and (d) 100 μM of Na_2HAsO_4, respectively. Six single-cell waveforms per group were recorded for each Na_2HAsO_4 concentration. The real impedance was normalized to the impedance value two hours prior to Na_2HAsO_4 inoculation ($t = 0$ h), and toxicant deposition was made at $t = 2$ h indicated by a faded vertical line. (e) Time course graphs of the averaged real impedance waveforms of T98G single cells exposed to 0, 10, 20, 50, and 100 μM of Na_2HAsO_4.

results from a previous study (where 60 μM showed no decline in cell impedance).[20]

Conclusions

In this study we demonstrated that single-cell impedance can be used to analyze cellular death resulting from cytotoxicity. The averaged real impedance response of individual T98G cells showed temporal- and concentration-dependent effects on H_2O_2, $NaAsO_2$, and Na_2HAsO_4 toxicants. The impedance waveforms of single cells revealed the diversity of individual cell responses indicative of morphological change throughout the entire experimental period. These measurements enabled the analysis of cell-to-cell variation in cytotoxic response, particularly prevalent at lower toxicant concentrations, which would have otherwise been lost in bulk cell population measurements. Using analytical modeling, important information regarding the mechanisms of cell death such as time constants of apoptosis and necrosis was derived. This approach of monitoring single-cell impedance demonstrated a number of advantages over conventional viability based assays including continuous-time recording and increased cell signal sensitivity, which holds great implications for future use in drug screening and toxicant detection for a wide range of biomedical and environmental applications.

Acknowledgements

The authors acknowledge the funding support from the National Institutes of Health (NIH/GMS) for the project of "Microelectrode arrays of single cell biosensors" (R01GM075095) and lab assistance of Solyvattey Malei.

References

1 K. Slater, *Curr. Opin. Biotechnol.*, 2001, **12**, 70–74.
2 K. Durick and P. Negulescu, *Biosens. Bioelectron.*, 2001, **16**, 587–592.
3 P. Banerjee and A. K. Bhunia, *Trends Biotechnol.*, 2009, **27**, 179–188.
4 E. Michelini, L. Cevenini, L. Mezzanotte, A. Coppa and A. Roda, *Anal. Bioanal. Chem.*, 2010, **398**, 227–238.
5 K. H. Vousden, *Cancer Cell*, 2002, **2**, 351–352.
6 J. Z. Xing, L. J. Zhu, J. A. Jackson, S. Gabos, X. J. Sun, X. B. Wang and X. Xu, *Chem. Res. Toxicol.*, 2005, **18**, 154–161.
7 J. El-Ali, P. K. Sorger and K. F. Jensen, *Nature*, 2006, **442**, 403–411.
8 W. An and N. Tolliday, *Mol. Biotechnol.*, 2010, **45**, 180–186.
9 J. M. Levsky and R. H. Singer, *Trends Cell Biol.*, 2003, **13**, 4–6.
10 F. Asphahani and M. Zhang, *Analyst*, 2007, **132**, 835–841.
11 L. Ceriotti, J. Ponti, P. Colpo, E. Sabbioni and F. Rossi, *Biosens. Bioelectron.*, 2007, **22**, 3057–3063.
12 C. Spegel, A. Heiskanen, L. H. D. Skjolding and J. Emneus, *Electroanalysis*, 2008, **20**, 680–702.
13 K. B. Male, S. M. Crowley, S. G. Collins, Y. M. Tzeng and J. H. T. Luong, *Anal. Methods*, 2010, **2**, 870–877.

14 L. Huang, L. Xie, J. M. Boyd and X. F. Li, *Analyst*, 2008, **133**, 643–648.
15 J. M. Boyd, L. Huang, L. Xie, B. Moe, S. Gabos and X. F. Li, *Anal. Chim. Acta*, 2008, **615**, 80–87.
16 T. M. Curtis, M. W. Widder, L. M. Brennan, S. J. Schwager, W. H. van der Schalie, J. Fey and N. Salazar, *Lab Chip*, 2009, **9**, 2176–2183.
17 K. B. Male, B. Lachance, S. Hrapovic, G. Sunahara and J. H. T. Luong, *Anal. Chem.*, 2008, **80**, 5487–5493.
18 M. Tarantola, D. Schneider, E. Sunnick, H. Adam, S. Pierrat, C. Rosman, V. Breus, C. Sonnichsen, T. Basche, J. Wegener and A. Janshoff, *ACS Nano*, 2009, **3**, 213–222.
19 E. Hondroulis, C. Liu and C. Z. Li, *Nanotechnology*, 2010, **21**, 9.
20 C. D. Xiao, B. Lachance, G. Sunahara and J. H. T. Luong, *Anal. Chem.*, 2002, **74**, 5748–5753.
21 C. Xiao and J. H. T. Luong, *Biotechnol. Prog.*, 2003, **19**, 1000–1005.
22 C. Xiao and J. H. T. Luong, *Toxicol. Appl. Pharmacol.*, 2005, **206**, 102–112.
23 E. Primiceri, M. S. Chiriaco, E. D'Amone, E. Urso, R. E. Ionescu, A. Rizzello, M. Maffia, R. Cingolani, R. Rinaldi and G. Maruccio, *Biosens. Bioelectron.*, 2010, **25**, 2711–2716.
24 J. H. Yeon and J. K. Park, *Anal. Biochem.*, 2005, **341**, 308–315.
25 A. Ahmad and E. J. Moore, *Anal. Lett.*, 2009, **42**, 1–28.
26 C. D. James, N. Reuel, E. S. Lee, R. V. Davalos, S. S. Mani, A. Carroll-Portillo, R. Rebeil, A. Martino and C. A. Apblett, *Biosens. Bioelectron.*, 2008, **23**, 845–851.
27 D. Malleo, J. T. Nevill, L. P. Lee and H. Morgan, *Microfluid. Nanofluid.*, 2010, **9**, 191–198.
28 F. Asphahani, K. Wang, M. Thein, O. Veiseh, S. Yung, J. Xu and M. Zhang, *Phys. Biol.*, 2011, **8**, 015006.
29 F. Asphahani, M. Thein, O. Veiseh, D. Edmondson, R. Kosai, M. Veiseh, J. Xu and M. Q. Zhang, *Biosens. Bioelectron.*, 2008, **23**, 1307–1313.
30 M. Veiseh, O. Veiseh, M. C. Martin, F. Asphahani and M. Q. Zhang, *Langmuir*, 2007, **23**, 4472–4479.
31 M. Thein, F. Asphahani, A. Cheng, R. Buckmaster, M. Q. Zhang and J. Xu, *Biosens. Bioelectron.*, 2010, **25**, 1963–1969.
32 M. K. Soliman, E. Mazzio and K. F. A. Soliman, *Life Sci.*, 2002, **72**, 185–198.
33 V. M. Rodriguez, M. E. Jimenez-Capdeville and M. Giordano, *Toxicol. Lett.*, 2003, **145**, 1–18.
34 Y. Kitamura, T. Ota, Y. Matsuoka, I. Tooyama, H. Kimura, S. Shimohama, Y. Nomura, P. J. Gebicke-Haerter and T. Taniguchi, *Glia*, 1999, **25**, 154–164.
35 M. Veiseh and M. Zhang, *J. Am. Chem. Soc.*, 2006, **128**, 1197–1203.
36 S. W. Ryter, H. P. Kim, A. Hoetzel, J. W. Park, K. Nakahira, X. Wang and A. M. K. Choi, *Antioxid. Redox Signaling*, 2007, **9**, 49–89.
37 L. Ceriotti, J. Ponti, P. Colpo, E. Sabbioni and F. Rossi, *Biosens. Bioelectron.*, 2007, **22**, 3057–3063.
38 Y. Okada, E. Maeno, T. Shimizu, K. Manabe, S. Mori and T. Nabekura, *Pflugers Arch.*, 2004, **448**, 287–295.
39 M. C. Willingham, *J. Histochem. Cytochem.*, 1999, **47**, 1101–1109.
40 G. R. Ding, T. Nakahara, H. Hirose, S. Koyama, Y. Takashima and J. Miyakoshi, *Int. J. Radiat. Biol.*, 2004, **80**, 317–324.
41 L. Bouchier-Hayes, C. Munoz-Pinedo, S. Connell and D. R. Green, *Methods*, 2008, **44**, 222–228.
42 Z. Dong, P. Saikumar, J. M. Weinberg and M. A. Venkatachalam, *Am. J. Pathol.*, 1997, **151**, 1205–1213.
43 L. F. Barros, T. Kanaseki, R. Sabirov, S. Morishima, J. Castro, C. X. Bittner, E. Maeno, Y. Ando-Akatsuka and Y. Okada, *Cell Death Differ.*, 2003, **10**, 687–697.